Journal of Nanobiotechnology

RESEARCH

Open Access

Multifunctional carbomer based ferulic acid hydrogel promotes wound healing in radiation-induced skin injury by inactivating NLRP3 inflammasome

Congshu Huang[1,3†], Chaoji Huangfu[1†], Zhijie Bai[1†], Long Zhu[4], Pan Shen[1], Ningning Wang[1], Gaofu Li[1], Huifang Deng[1], Zengchun Ma[1*], Wei Zhou[1*] and Yue Gao[1,2*]

Abstract

Background Radiation-induced skin injury is a significant adverse reaction to radiotherapy. However, there is a lack of effective prevention and treatment methods for this complication. Ferulic acid (FA) has been identified as an effective anti-radiation agent. Conventional administrations of FA limit the reaching of it on skin. We aimed to develop a novel FA hydrogel to facilitate the use of FA in radiation-induced skin injury.

Methods We cross-linked carbomer 940, a commonly used adjuvant, with FA at concentrations of 5%, 10%, and 15%. Sweep source optical coherence tomography system, a novel skin structure evaluation method, was applied to investigate the influence of FA on radiation-induced skin injury. Calcein-AM/PI staining, CCK8 assay, hemolysis test and scratch test were performed to investigate the biocompatibility of FA hydrogel. The reducibility of DPPH and ABTS radicals by FA hydrogel was also performed. HE staining, Masson staining, laser Doppler blood flow monitor, and OCT imaging system are used to evaluate the degree of skin tissue damage. Potential differentially expressed genes were screened via transcriptome analysis.

Results Good biocompatibility and in vitro antioxidant ability of the FA hydrogels were observed. 10% FA hydrogel presented a better mechanical stability than 5% and 15% FA hydrogel. All three concentrations of FA remarkably promoted the recovery of radiation-induced skin injury by reducing inflammation, oxidative conidiation, skin blood flow, and accelerating skin tissue reconstruction, collagen deposition. FA hydrogel greatly inhibiting the levels of NLRP3, caspase-1, IL-18, pro-IL-1β and IL-1β in vivo and *vitro* levels through restraining the activation of NLRP3

†Congshu Huang, Chaoji Huangfu and Zhijie Bai contributed equally to this work.

*Correspondence:
Zengchun Ma
mazchun@139.com
Wei Zhou
zhouweisyl802@163.com
Yue Gao
gaoyue@bmi.ac.cn

Full list of author information is available at the end of the article

inflammasome. Transcriptome analysis indicated that FA might regulate wound healing via targeting immune response, inflammatory response, cell migration, angiogenesis, hypoxia response, and cell matrix adhesion.

Conclusions These findings suggest that the novel FA hydrogel is a promising therapeutic method for the prevention and treatment of radiation-induced skin injury patients.

Keywords Ferulic acid, Radiation-induced skin injury, NLRP3 inflammasome

Graphical Abstract

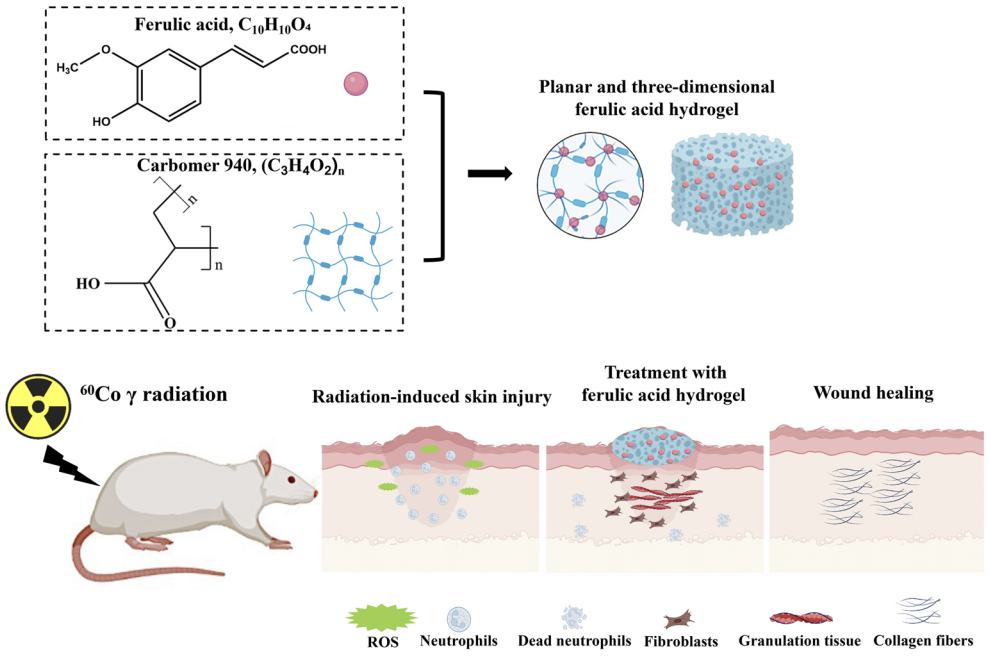

Introduction

Radiotherapy is widely used as a routine treatment method in tumor treatment. However, radiotherapy often leads to radiation-induced skin injury, which is characterized by long-lasting, recurring, and difficult-to-heal wounds [1, 2]. Radiotherapy alone or as an adjunctive treatment of surgery is one of the most effective treatments for head, neck, skin, anal, and breast cancers [3, 4]. Approximately 95% of patients taking radiotherapy in clinical experience radiation-induced skin injury [5]. Radiation-induced skin injury limits the further application of radiotherapy in tumor treatment and has a significant negative impact on the quality of life and treatment of patients [6, 7]. Currently, apart from conservative treatment, there are no effective preventive measures or treatment methods available [8]. Therefore, seeking effective prevention and treatment measures for radiation-induced skin injury is necessary.

Ferulic acid (FA) is a naturally occurring antioxidant in plant cell walls, not only present in the bran of gramineous plants such as wheat, rice, and oats, but also an effective component of traditional Chinese medicine such as *Angelicae Sinensis Radix* and *Chuanxiong Rhizoma* [9–11]. FA, as an anti-oxidant, not only has strong high antioxidant and anti-inflammatory activity, but also presents anti-radiation effects [12]. FA can improve the activity of superoxide dismutase and achieve antioxidant effect by inhibiting the production of reactive oxygen species (ROS) in the body [13]. The protective effect of FA depends on dietary intake, but the obvious first pass elimination causes the oxidation and destruction of most FA, thus reducing its plasma concentration and skin residual amount, which limits the application of FA in radiation-induced skin injury [14].

Hydrogels has the advantages of non-greasy, fast release, comfortable lubrication, easy spread, and non-irritating to skin and mucosa [15]. It is suitable for skin diseases and has unique advantages in combination with traditional Chinese medicine [16, 17]. Carbomer is an excellent new type of medicinal excipient, and it is widely used in the research and production of cosmetics and drugs. Carbomer is mainly used as a matrix of thickener, suspension aid, and adhesive in pharmaceuticals [18]. A combined cyanine/carbomer gel has been used in wound healing by promoting anti-microbial activity [18]. Ångstrom-scale silver particle-embedded carbomer gel accelerates wound healing via suppressing bacterial colonization and inflammation [19]. The studies suggest that

carbomer is an ideal matrix for hydrogel preparation. FA embedder carbomer hydrogel has not been reported, and this kind of gel might directly deliver FA to radiation-induced skin injury sites.

Radiation can cause a large number of free radicals in the skin, increase the apoptosis rate of skin cells, and lead to oxidative damage reactions [20]. Skin injury could further lead to the activation of the body's immune system and the release of inflammatory factors [21]. During this process, NLRP3 inflammasomes are activated and further activate the self-catalytic caspase-1, causing the increase of NLRP3, and the downstream inflammatory factors, IL-18 and IL-1β [22]. Currently, reports on the role of NLRP3 inflammasomes in wound healing are inconsistent. It was reported that Lactobacillus Plantarum promoted diabetic foot wound healing by inhibiting the NLRP3 Inflammasomes [23]. Sustained activation of NLRP3 inflammasomes impair wound healing of diabetic foot ulcers [24]. However, knocking out NLRP3 slows down wound healing, and NLRP3 is protective in burn wound healing [25]. This indicates that the role of NLRP3 inflammasomes in wound healing is complex, which may be related to the type of wound and different stages of wound healing. The role of NLRP3 inflammasomes in radiation-induced skin injury has not been reported. If FA hydrogel could improve radiation-induced skin injury by regulating NLRP3 inflammasome remains unclear.

In this study, carbomer hydrogel combined with different concentration of FA was prepared to mitigate radiation-induced skin injury. We concluded that the novel FA hydrogel might improve radiation-induced skin injury through inactivating NLRP3 inflammasome. FA embedded carbomer hydrogel might be a novel promising therapeutic strategy for the treatment of radiation-induced skin injury patients.

Materials and methods

Preparation of FA embedded carbomer hydrogel

The three concentrations (5%, 10%, and 15%) of FA embedded carbomer hydrogels were prepared as follows. Firstly, 0.75 g of carbomer 940 (#C832684, Shanghai Macklin Biochemical Technology Co., Ltd, Shanghai, China) was dispersed in 85 mL, 80 mL, and 75 mL of distilled water, respectively, and allowed to swell for 24 h. Glycerol (5 g) and ethyl p-hydroxybenzoate (0.001 g) were added to the carbomer 940 gels at different concentrations. After thorough stirring and mixing, 5 g, 10 g, and 15 g of FA (#F809521, $C_{10}H_{10}O_4$, purity > 99.99%, Shanghai Macklin Biochemical Technology Co., Ltd, Shanghai, China) were added to the carbomer 940 gels of different concentrations, respectively. The pH value was adjusted to 5.5 using triethanolamine (#90279, Sigma-Aldrich, US). This process resulted in the preparation of 5%, 10%, and 15% FA-embedded carbomer hydrogels.

Characterization of FA embedded carbomer hydrogel

The particle size analysis was conducted as follows: the FA gel sample (1 mL) was placed in a 5 mL centrifuge tube and mixed with 2 mL of ethanol. The samples were dispersed by ultrasonication for 5 min, and then 1 mL of the upper layer solution was transferred to a sample cell for particle size measurement using the Marvin laser particle size analyzer (ZS90). Transmission electron microscopy (TEM) analysis was performed as follows: The FA gel sample was dispersed in ethanol, following the same procedure as mentioned above. The resulting sample solution was placed onto an ultra-thin carbon film and air-dried. TEM imaging was carried out using the FEI Tecnai G2F30 microscope operating at an acceleration voltage of 200 kV. Rheological properties were measured using a rotational rheometer (#MCR92, Anton Paar, Austria) following a previously described protocol [26]. An oscillatory strain amplitude sweep was performed with a strain range from 0.1 to 1000% at a frequency of 1 Hz and a temperature of 25 °C. Subsequently, a shear strain of 0.2% was applied, and an oscillatory frequency sweep ranging from 0.1 to 100 rad/s was conducted at 25 °C. The model of the test rotor was a parallel plate of 50 mm, with a gap setting of 1 mm.

The swelling detection of FA hydrogels was performed as described below. The dry FA hydrogels (W1) were immersed in phosphate buffered saline (PBS), and removed at 2, 4, 6, 8 h. After removing water with filter paper, the weights of FA hydrogels were recorded (W2). The swelling ratio= [(W2-W1)/W1]×100%.

In vitro antioxidant ability of of FA hydrogels

The scavenging abilities of 2,2'-azinobis (3-ethylbenzothiazoline)-6-sulfonic acid (ABTS) radicals, 1,1-diphenyl-2-picrylhydrazyl (DPPH) radicals, and ROS production by FA hydrogels were investigated as described previously [27]. To evaluate the hydrogel's ability to scavenge DPPH radicals, FA hydrogels (200 μL) were prepared in a 24-well plate and immersed in 1 mL of anhydrous ethanol. DPPH solution dissolved with 0.5 mM ethanol was added. After incubation for 1 h in the darkness, OD value at 517 nm was measured (OD_{FA}). PBS was added instead of FA hydrogels for control (OD_{Con}). The scavenging efficiency of DPPH radicals = [(OD_{Con} - OD_{FA})/$OD_{Positive}$]×100%.

The scavenging ability of ABTS radicals was measured as described below. The FA hydrogels were incubated with ABTS working solutiong for 1 h in the dark. The OD value at 734 nm was measured. The scavenging efficiency of ABTS radicals = [(OD_{Con} - OD_{FA})/$OD_{Positive}$]×100%.

The HaCaT cells were treated with 100 μM hydrogen peroxide (H_2O_2) for 4 h to establish cell damage model. FA hydrogel extraction solutions were obtained by immersing hydrogel in DMEM/F12 for 24 h at 37 °C.

Then, medium containing H_2O_2 was replaced with FA hydrogel extraction solutions, or DMEM/F12 medium. After incubation for 24 h, DCFH-DA probe was added. After incubation for 30 min in the dark, cells were washed with PBS twice, and fluorescence intensity was observed by fluorescence microscopy.

Animal model establishment of radiation-induced skin injury

A ^{60}Co γ radiation source (Beijing Institute of Radiation Medicine, Beijing, China) was utilized to induce skin injuries. The animal experiments were performed in accordance with national and institutional guidelines. The experimental protocol was approved by the Ethics Committee of Animal Experiments of the Beijing Institute of Radiation Medicine (Approval number: IACUC-DWZX-2020-773). Seventy-two female Wistar rats (190–210 g, Beijing Weitong Lihua Experimental Animal Technology Co., Ltd, China) were randomly divided into six groups, including control, 40 Gy irradiation, 40 Gy irradiation + Aloe gel, 40 Gy irradiation + 5% FA gel, 40 Gy irradiation + 10% FA gel, and 40 Gy irradiation + 15% FA gel, with 12 rats in each group. The rats were housed under controlled conditions at a temperature of 22 ± 2 °C, a humidity of 50% ± 5%, and provided with sterilized feed and purified water ad libitum. After 1 week of acclimatization, the rats were used for the experiments. Anesthesia was induced using 1% pentobarbital sodium at a dosage of 40 mg/kg. The fur on the buttocks and back of the rats was shaved, and the rats were immobilized on an irradiation board. The buttocks and back of the rats in the experimental groups were exposed to a single dose of 40 Gy irradiation (266.24 cGy/min), while the rest of their bodies were shielded with lead bricks (Supplementary Fig. 1). After irradiation, the rats in the group 40 Gy irradiation, 40 Gy irradiation + Aloe gel, 40 Gy irradiation + 5% FA gel, 40 Gy irradiation + 10% FA gel, and 40 Gy irradiation + 15% FA gel were topically treated with carbomer hydrogel without FA, Aloe gel, 5% FA gel, 10% FA gel, and 15% FA gel, respectively, twice a day for 10 consecutive days. The weights of the animals were recorded on days 0, 7, 14, 21, and 28 after irradiation. The skin changes in the irradiated areas were observed daily after irradiation, and parameters such as peeling, redness, damage, and exudation were recorded. The degree of radiation-induced skin damage was analyzed using the Douglas and Fowler scores (Supplementary Table 1). On the 14th, 21st, and 28th days after radiation, skin tissues from the buttocks and back were collected for further analysis based on previous reports [27, 28]. Pentobarbital sodium (150 mg/kg) intraperitoneal injection was used to euthanize rats.

Hematoxylin and eosin (HE) staining

Skin tissue samples measuring 1 cm × 1 cm were collected from the buttocks and back areas and fixed in 4% paraformaldehyde. The tissues were then embedded in paraffin. The sections were dewaxed using the following steps: incubation in xylene for 15 min, anhydrous ethanol for 5 min, 85% alcohol for 5 min, and 75% alcohol for 5 min, in that order. Subsequently, the sections were stained with hematoxylin for 5 min and eosin for 30 s. After staining, the slices were immersed in anhydrous ethanol for 5 min, followed by incubation in xylene for 5 min, and finally sealed with transparent neutral gum.

Masson staining

The sections were stained with hematoxylin for 5 min. After washing with tap water, the tissues were differentiated with 1% hydrochloric acid alcohol for 3 s and rinsed with running water for 3 min. Acid fuchsin solution was used to stain the sections for 5 min, and phosphomolybdic-phosphotungstic acid was used to incubate the slides for 5 min. After incubating with aniline blue solution for 5 min, the sections were differentiated with 1% glacial acetic acid for 1 min. After dehydration, the slides were sealed with neutral gum and observed using an inverted microscope (Olympus, Japan). Pathological sections of three animals in each group were selected for Masson staining. Three random fields of each section were used to calculate the collage deposition ratio with Image J software. Collagen deposition = (collagen tissue area/whole tissue area)×100%.

Immunofluorescence staining

The sections were placed in EDTA solution (Servicebio, Wuhan, China) and heated for 8 min in a microwave for antigen repair. Afterward, the sections were washed with PBS and incubated with bovine serum albumin for 30 min to block nonspecific binding. Following the removal of bovine serum albumin, the sections were incubated with primary antibodies overnight at 4 °C and washed with PBS three times (5 min each time). The sections were then incubated with secondary antibodies for 1 h. After washing with PBS, the sections were incubated with DAPI solution (Servicebio, Wuhan, China) for 1 min. Finally, the sections were observed using a fluorescence microscope (Nikon, Japan). The antibodies used in this research are listed in supplementary Table 2.

Detection of skin blood flow using laser doppler blood flow monitor

Laser Doppler technology can be employed to monitor the blood perfusion of capillaries, venules, arterioles, and anastomotic branches in the skin, thereby reflecting changes in blood flow and the degree of skin damage. Rats were first anesthetized, and the skin blood flow

was recorded using a laser Doppler blood flow monitor (Moor Instruments, UK) on the 14th, 21st, and 28th days after radiation.

Evaluation of radiation-induced skin injury based on sweep source-OCT

Sweep-source optical coherence tomography (OCT) systems can be used to observe radiation-induced skin injury in real-time. This method enables non-invasive and radiation-free imaging [29]. By calculating and visualizing the optical attenuation coefficient, both qualitative and quantitative analysis of radiation-induced skin injury can be achieved. Wistar rats were anesthetized with 1% pentobarbital sodium on the 14th, 21st, and 28th days after irradiation, and the lesion site was scanned and analyzed. A sweep-source OCT system (Thorlabs, US) was used for three-dimensional reconstruction and quantitative analysis of skin damage.

Detection of inflammatory factors in the serum

The whole blood from the abdominal aorta were collected with a sterile injection syringe. After natural coagulation of blood at room temperature for 15–20 min, the blood samples were centrifuged at 4000 rpm/min at 4 °C for 20 min. The serum was extracted for the detection of inflammatory factors using the ELISA method according to the instructions. The Caspase-1, NLRP3, IL-1β, and IL-18 ELISA kits were purchased from Jiangsu Meimian Industrial Co., Ltd (Nanjing, Jiangsu province, China).

Cell culture and radiation-induced cell injury

The HaCaT cell line, a type of human keratinocyte, was used in this study. The cells were cultured using DMEM/F12 medium (Gibco) containing 10% fetal bovine serum (Gibco) and 1% penicillin-streptomycin (Gibco) at 37 °C with 5% CO_2. The cells were treated with radiation at a total dose of 18 Gy (100.68 cGy/min). FA solutions (200 μg/mL) were prepared using DMSO and diluted with DMEM/F12 to concentrations of 200, 100, 50, and 25 μg/mL. After radiation, the cell medium was replaced with different concentrations of FA solution or vitamin C solution (25 μg/mL, #A4403, Sigma-Aldrich, US). After 24 h of incubation, cells were used for detection.

ROS detection

The DCFH-DA probe (#D399, Thermo Fisher, US) was diluted with DMEM/F12 medium to a final concentration of 10 μmol/L. The irradiated cells were washed three times with PBS (#10010023, Thermo Fisher, US). Then, the DCFH-DA probe was added, and cells were incubated for 20 min in a 37 °C cell incubator. The supernatant was discarded, and cells were washed three times with DMEM/F12 medium. Flow cytometry was used to measure ROS intensity.

SOD detection

After removing the cell medium, the cells were scraped off with a cell scraper. The cells were then centrifuged at 2000 g for 10 min at 5 °C, and the supernatant was removed. The cells were washed twice with PBS. Ultrasound treatment of cells was performed on an ice bath. The cells were then centrifuged at 10,000 g for 15 min at 4 °C, and the supernatant was transferred to a new test tube. The prepared sample solution was used for SOD detection according to the instructions of the kit (Beiren Chemical Technology Co., Ltd, Japan).

CCK8 assay

To each well, 10 μL of CCK8 reagent (Beiren Chemical Technology Co., Ltd, Japan) was added. After incubation for 4 h at 37 °C in a 5% CO_2 incubator, the absorbance value at 450 nm was measured. The formula for cell viability is $[(OD_{FA} - OD_{Blank}) / (OD_{Con} - OD_{Blank})]\times100\%$.

Western blotting

Proteins from the skin tissues and cells were isolated using lysate containing RIPA lysate, protease inhibitor, and phosphatase inhibitor. The protein concentration was determined using the bicinchoninic acid (BCA) assay. Approximately 30 μg of proteins were loaded and separated through SDS-PAGE. The proteins were then transferred to a Polyvinylidene fluoride (PVDF) membrane (Millipore) at 100 mA current for 150 min. The membrane was blocked with tris buffered saline with tween (TBST) containing 5% skim milk. After washing with TBST, the membrane was incubated with primary antibodies overnight at 4 °C. Secondary antibodies were used to incubate the membranes at room temperature for 2 h, followed by washing with TBST. The proteins were detected using the Image Quant Las 500. The antibodies used in this research are listed in supplementary Table 2.

Transcriptome sequencing

The assessment of RNA purity and integrity was conducted utilizing a NanoPhotometer spectrophotometer and an Agilent 2100 bioanalyzer, respectively. For the construction of libraries, the NEBNext® Ultra™ RNA Library Prep Kit for Illumina was utilized. Quantification was initially undertaken with a Qubit 2.0 Fluorometer, and the insert size was subsequently evaluated using the Agilent 2100 bioanalyzer. The determination of the library's effective concentration was achieved through qRT-PCR. The library amplification process involved the integration of fluorescently-labeled dNTPs, DNA polymerase, and adapter primers. During the extension phase of each sequencing cluster, fluorescently-labeled dNTPs were incorporated, triggering the emission of corresponding fluorescence signals. The calculation of FPKM (Fragments per kilo base per million mapped reads)

values for individual genes was based on gene length and the number of mapped reads. The analysis of differential expression across comparison groups was performed employing DESeq2 software, with the adjustment of P-values according to the Benjamini & Hochberg method [30]. Criteria for significant differential expression were established by adjusted P-values and the magnitude of |log2foldchange|. Differentially expressed genes were analyzed functionally using Kyoto Encyclopedia of Genes and Genomes (KEGG) and Gene Ontology (GO) with the Database for Annotation, Visualization and Integrated Discovery (DAVID) tool. The thresholds for Padj < 0.05 and FDR < 0.05 were applied.

Statistical analysis

All experimental data were obtained by independently repeating the experiments at least three times. The experimental data were presented as mean ± SD and analyzed using GraphPad 8 software. A t-test was conducted to compare data between two groups, and ANOVA was used to compare data among multiple groups, with $P < 0.05$ indicating significant statistical differences.

Results

Characterization of FA hydrogel

The prepared hydrogels exhibited a uniform and delicate appearance, maintained a gelatinous state at room temperature, did not dry out, had no bubbles, and demonstrated good ductility, meeting the quality standards of gel as described in the Chinese Pharmacopoeia (Part III) [31]. The morphology of 5%, 10%, and 15% FA hydrogels was observed using TEM. The FA hydrogels exhibited a round morphology, and they were well cross-linked together (Fig. 1A). The diameter of a single gel bead was approximately 50 nm (Fig. 1A). The size of the cross-linked gels increased with the concentration of FA (Fig. 1B): 5% FA cross-linked gels: 583.6 ± 12.7 nm, 10% FA cross-linked gels: 718.9 ± 22.8 nm, 15% FA cross-linked gels: 876.4 ± 15.4 nm. The storage modulus (G') of the hydrogel was higher than the loss modulus (G") at all oscillation frequencies, indicating that the FA hydrogel with different concentrations had good mechanical properties. Specifically, the G' of the 10% FA hydrogel was higher than that of the 5% FA hydrogel and the 15% FA hydrogel, suggesting that the mechanical strength of the hydrogel increased with the FA concentration, although a concentration of 15% FA affected the cross-linked network (Fig. 1C). The G' of the 5%, 10%, and 15% FA gels remained relatively constant from 0.1–4.6% shear strain and decreased significantly from 10–1000% strain (Fig. 1D). The 10% FA gel exhibited the highest G' compared to the 5% and 15% FA gels, which was consistent with the results obtained from the oscillation frequency measurement (Fig. 1C). As time goes on, the swelling rate gradually decreased, but there was no significant difference among the three groups (Fig. 1E).

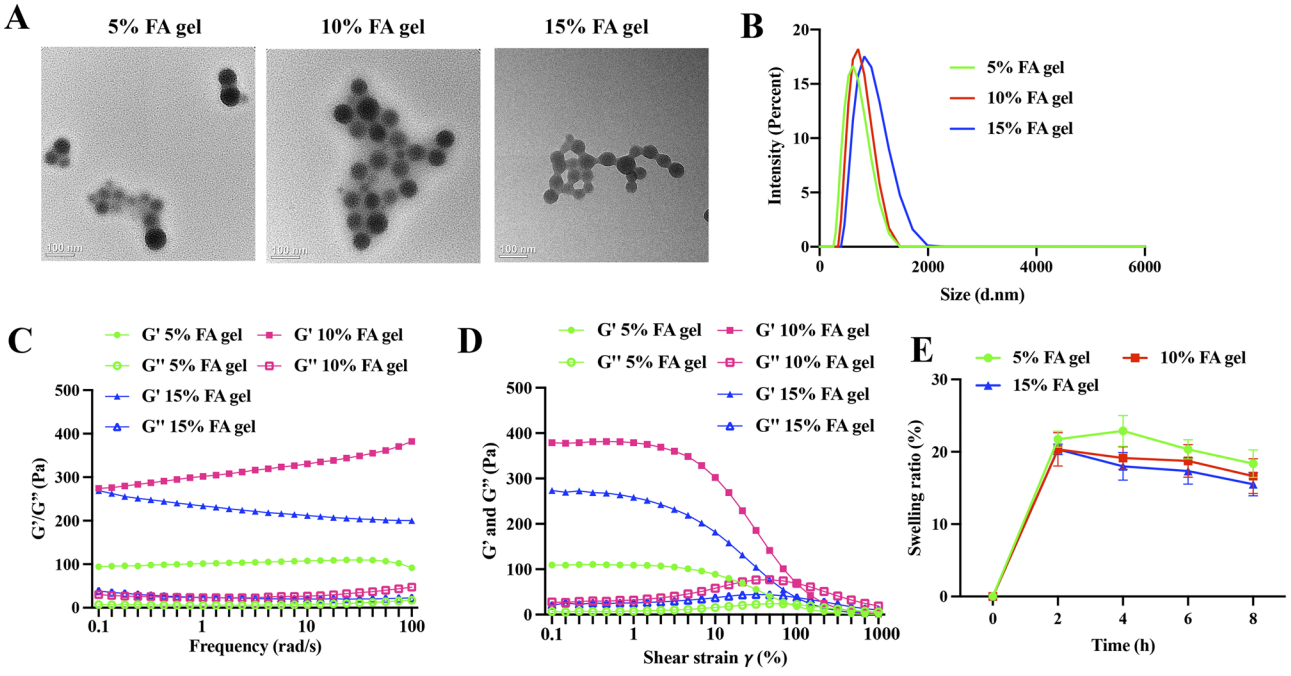

Fig. 1 Characterization of FA hydrogel. (**A**) Representative morphology of FA gel observed by TEM. (**B**) Particle size analysis of FA gel. (**C**) Rheological analysis of the hydrogels in oscillatory frequency sweep mode. (**D**) Rheological analysis of the hydrogels in oscillatory stress response mode. (**E**) The swelling ratio of three groups was presented

Biocompatibility of the FA hydrogels

The biocompatibility of the FA hydrogels was evaluated by measuring cell viability through CCK8 assay and calcein-AM/PI staining. After incubating for 24, 48, and 72 h with three FA concentration hydrogel extracts, HaCaT living cells accounted for the largest number, and red fluorescent dead cells were very rare, which showed that FA hydrogel was non-toxic to HaCaT cells (Fig. 2A). The results of CCK8 assay also confirmed the above results. After 24, 48 and 72 h of incubation with FA hydrogel extract, the cell viability was still about 100% (Fig. 2B). The migration of fibroblasts is crucial for wound healing. We further investigated the effect of FA hydrogel on fibroblast migration. The results showed that after 24 h incubation with FA hydrogel extract, the migration ability of fibroblasts had no significant difference compared with the control group (Fig. 2C). In addition, the blood compatibility of FA hydrogels was also investigated. The hemolysis ratios of 5%, 10%, and 15% FA hydrogels were 3.73±0.46, 4.1±0.36, 4.68±0.86, respectively (Fig. 2D), which meet the the standard of <5% (ISO 10993-4). These findings suggest that FA hydrogels have good biocompatibility.

In vitro antioxidant ability of of FA hydrogels

After radiation, the skin produces a large amount of ROS, which can aggravate tissue damage and hinder wound healing. We investigated the scavenging capacity of FA hydrogel for ROS at the cellular level. Large amount of ROS in the HaCat cells were induced by H_2O_2. However, after incubation with FA hydrogels, the fluorescence intensity was greatly decreased, suggesting that FA hydrogels could effectively scavenge ROS (Fig. 3A). The scavenging ability of ABTS and DPPH is also the representative index for evaluation of the antioxidant efficiency. We found that 3 concentrations of FA hydrogels significantly decreased the levels of both ABTS (Fig. 3B) and DPPH (Fig. 3C). These findings suggest that FA hydrogels have good antioxidant ability.

FA gel significantly accelerated the recovery of radiation-induced skin injury

Continuous treatment on the skin of rats for 72 h confirmed that FA hydrogel had no skin irritation (Supplementary Fig. 2). The animal experiment plan is illustrated in Fig. 4A. Rats exposed to radiation exhibited a small amount of erythema on the skin on the 7th day after irradiation, which progressed to peeling and redness of varying degrees on the 14th day. On the 21st day, the damage worsened, resulting in ulcers, bleeding, and necrosis (Fig. 4B). According to the Douglas and Fowler radiation dermatitis scoring criteria, the skin injury of the rats was evaluated on days 1, 3, 5, 7, 14, 21, and 28 after irradiation. The highest score was observed on the 21st day in the group exposed to 40 Gy, indicating the most severe skin damage on that day (Fig. 4B). On the 21st and 28th days after irradiation, the radiation dermatitis scores in the FA gel treatment groups were significantly lower than those in the 40 Gy group (Fig. 4C), suggesting that FA gel had a therapeutic effect on radiation-induced skin damage. During the first 7 days after radiation, rats exhibited a decrease in appetite and a gradual decrease in weight, indicating that ^{60}Co γ had a significant impact on the weight of rats in the early stages after irradiation

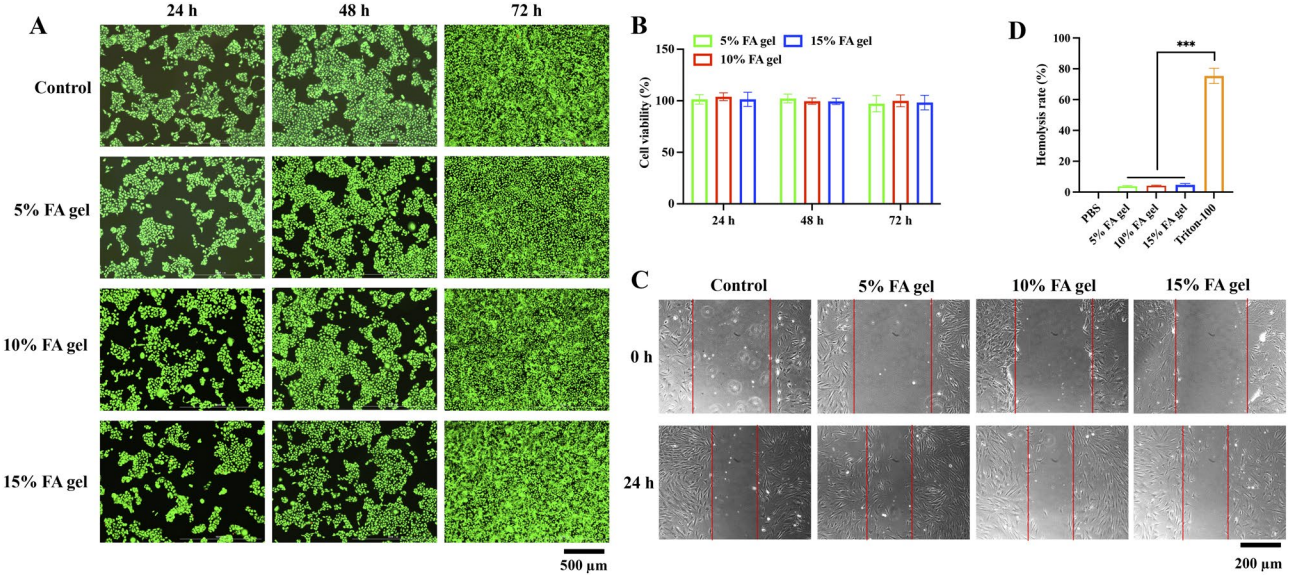

Fig. 2 The evaluation of FA hydrogels biocompatibility. (**A**) Calcein-AM/PI staining of HaCaT cells after incubation with FA hydrogels extracts for 24, 48, and 72 h. (**B**) The cell viability was measured via CCK8 assay after incubation with FA hydrogels extracts for 24, 48, and 72 h. (**C**) The migration of fibroblast was evaluated with wound healing assay. (**D**) The hemolysis ratios of FA hydrogels were evaluated. *** $p < 0.001$ compared with group Triton-100

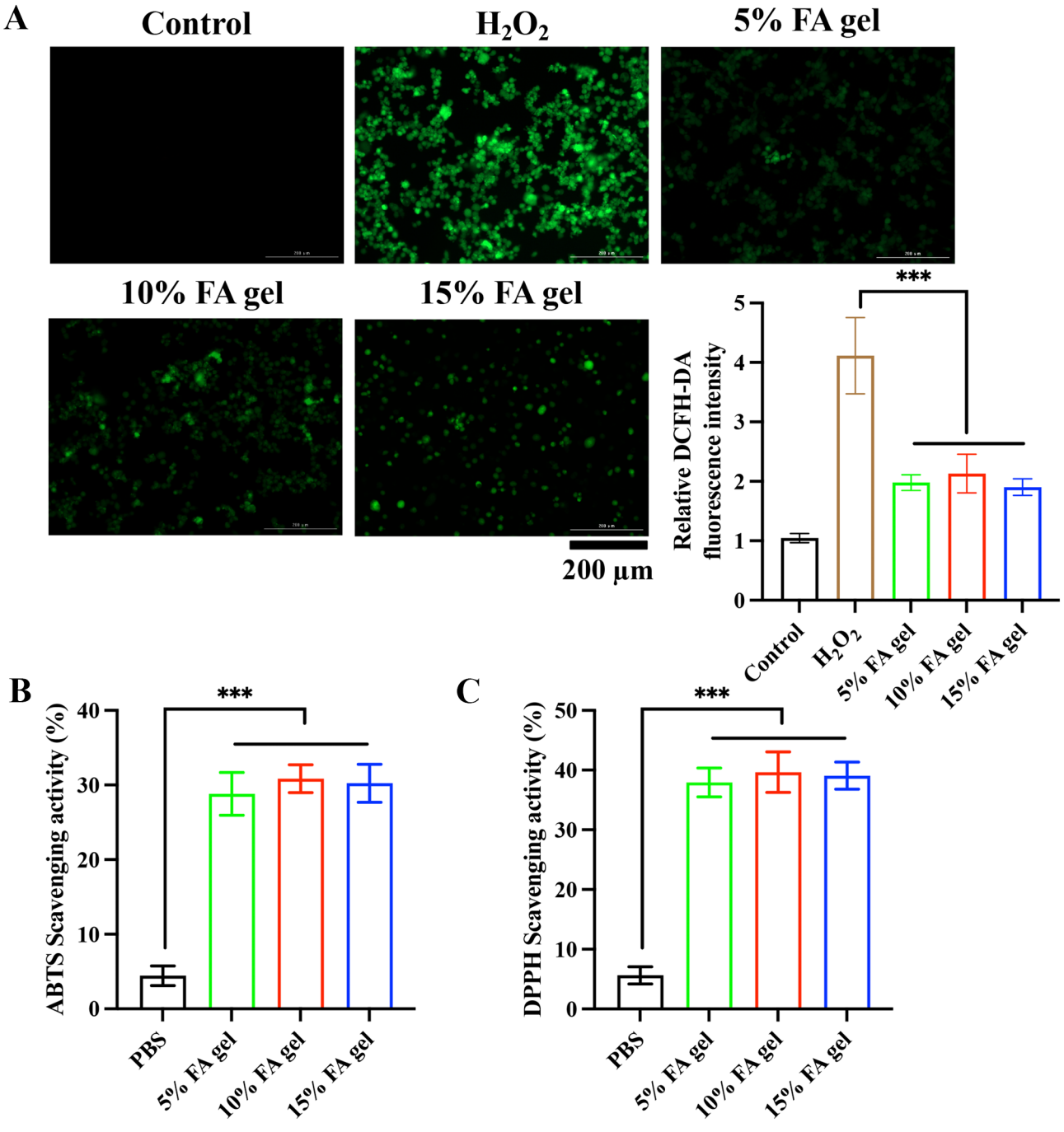

Fig. 3 In vitro antioxidant ability of of FA hydrogels. (**A**) The level of ROS in HaCaT cells was evaluated with DCFH-DA staining method. (**B**-**C**) The scavenging activities of ABTS radicals and DPPH radicals were evaluated. *** $p < 0.001$

(Fig. 4D). On the seventh day after irradiation, the weight of rats stabilized and showed a slow increasing trend. However, no significant difference was observed among the different irradiation groups (Fig. 4D).

Additionally, the skin injury was evaluated through HE staining (Fig. 4E). On the 14th, 21st, and 28th days after irradiation, the skin layer structure of the normal group rats remained normal, with normal morphology and structure of hair follicles, sebaceous glands, and sweat glands in the dermis. No congestion or inflammatory cell infiltration was observed in the subcutaneous blood vessels (Fig. 4E). On the 21st day after irradiation, a large number of inflammatory cells infiltrated the dermis tissue of rats in the 40 Gy group, and collagen fibers in the dermis were damaged. On the 28th day after irradiation, the epidermal layer of rats in the 40 Gy group

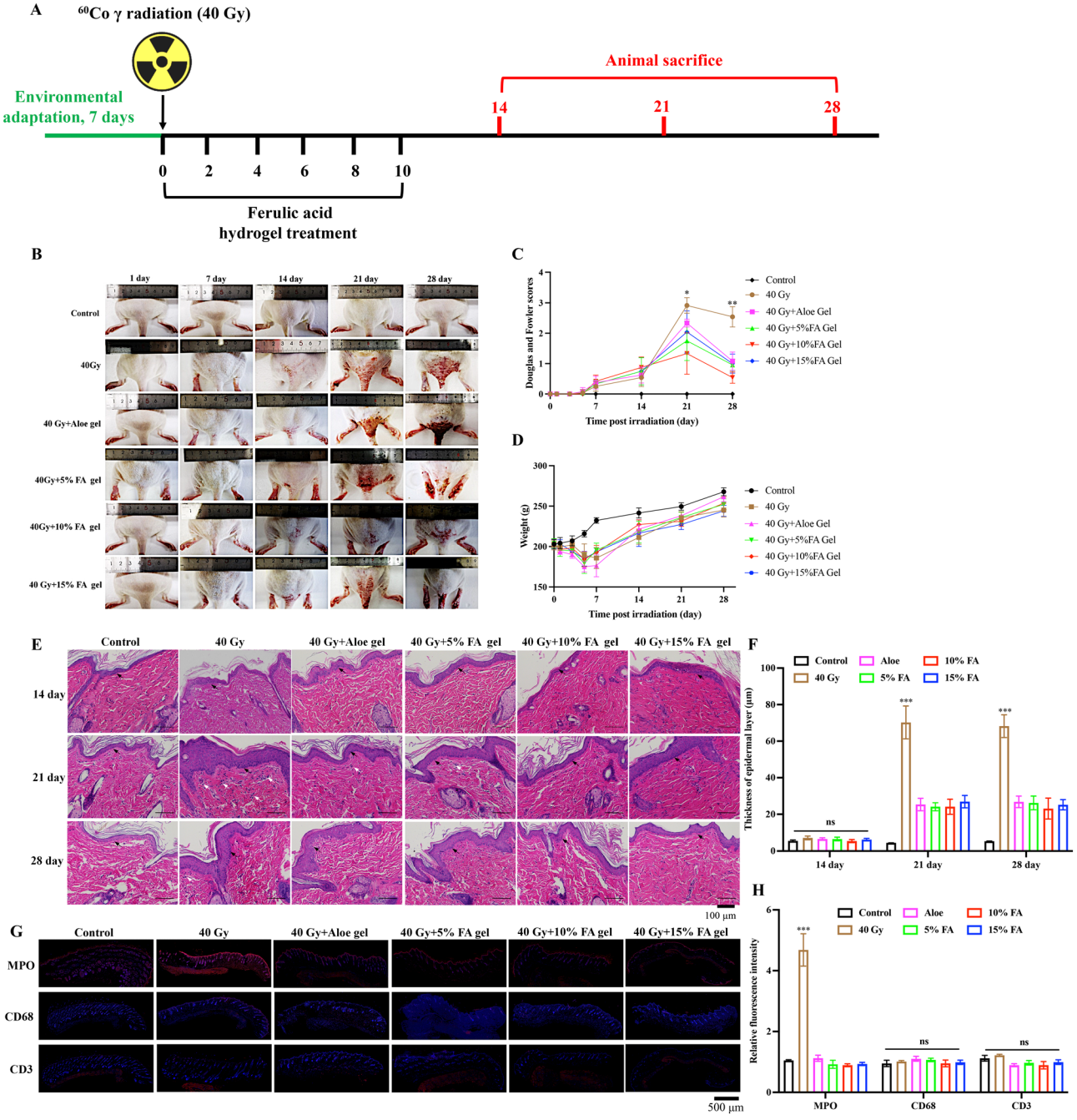

Fig. 4 FA hydrogels accelerates the recovery of radiation-induced injury. (**A**) Progression of radiation-induced animal model establishment and FA gel administration. (**B**) Gross images of rat skin on the buttocks and back. (**C**) Evaluation of skin injury using the Douglas and Fowler score. (**D**) Recording of rat weight. (**E**) Histological analysis of skin tissues using HE staining (Black arrows indicate keratinization layer, and white arrows indicate inflammatory cells). (**F**) Detection of thickness of epidermal layer. (**G**-**H**) The fluorescence intensity of MPO, CD68, and CD3 in dermis and epidermis were evaluated. * $p < 0.05$, ** $p < 0.01$, *** $p < 0.01$ compared with the 40 Gy + Aloe gel, 40 Gy + 5% gel, 40 Gy + 10% gel, 40 Gy + 15% gel groups

significantly thickened, keratinization worsened, and the structures of accessory organs such as sweat glands, hair follicles, and sebaceous glands were damaged, with a decrease in the number of skin appendages (Fig. 4E). On the 14th day after irradiation, different concentrations of FA gel delayed the onset of skin damage by decreasing inflammatory cells infiltration and epidermal layer thickness. On the 21st day after irradiation, FA gel significantly reduced the degree of radiation-induced skin damage by alleviating damage of sweat glands, hair follicles, and suppressing inflammatory response. On the 28th day after irradiation, FA gel significantly reduced skin edema,

increased granulation tissue proliferation, and inhibited inflammatory cell infiltration (Fig. 4E). We also find that significant the increase of epidermal layer thickness induced by radiation was greatly decreased by FA hydrogel (Fig. 4F). We performed immunofluorescence staining for markers of neutrophils (MPO), macrophages (CD68), and T cells (CD3), and found that the expression of neutrophils was significantly higher after radiation, and the treatment of FA hydrogel significantly inhibited the infiltration of neutrophils (Fig. 4G-H). However, there was no difference in the expression intensity of macrophages and T cells among different groups. (Fig. 4G-H). No significant difference was observed between FA-treated groups and Aloe-treated group in weight, thickness of epidermal layer, and the fluorescence intensity of MPO, CD68, CD3 (Fig. 4).

FA gel greatly reduced rat skin blood flow and promoted skin tissue reconstruction after radiation

Skin blood flow can increase after skin damage. There was no significant difference in skin blood flow changes in the normal group on the 14th, 21st, and 28th days (Fig. 5A-B). Rats in the 40 Gy group exhibited increased skin blood flow, with the highest perfusion observed on the 21st day, which may be related to skin swelling and inflammatory reactions. Compared to the 40 Gy group, treatment with aloe gel slowed down the time and degree of increased skin blood flow (Fig. 5A-B). Furthermore, treatment with 5%, 10%, and 15% FA gel significantly decreased the areas of redness, swelling, and blood flow in the skin (Fig. 5A-B).

The OCT imaging system enabled the observation of skin structural information up to a depth of 1.5 mm. In the 40 Gy group, the area and depth of skin damage increased markedly, and disordered tissues were observed after radiation. However, different concentrations of FA gel exhibited a protective effect on the skin structure of rats, resulting in lower structural damage to the rat skin after irradiation and faster recovery (Fig. 5C-D). Additionally, higher collagen deposition and a visible ordered collagen fiber array were observed after treatment with 10% or 15% FA gel compared to the 40 Gy group (Fig. 5E-F). The treatment of Aloe gel and 5% FA also improved the collagen fiber structure, but the increase of collagen deposition in groups 40 Gy+Aloe gel and 40 Gy+5% FA gel was not significant compared with group 40 Gy (Fig. 5E-F). Meanwhile, no significant difference was observed between FA-treated groups and Aloe-treated group (Fig. 5E-F).

FA gel remarkably suppressed the activation of NLRP3 inflammasome caused by 40 gy in vivo

The activation of the NLRP3 inflammasome and the subsequent increase in inflammatory response were observed on the 21st and 28th days after 40 Gy radiation. After 40 Gy irradiation, the expression of NLRP3 (Fig. 6A) and downstream inflammation factors, caspase-1, IL-1β, and IL-18, and pro-IL-1β (Fig. 6B-E) in the serum significantly increased. However, the increased levels of NLRP3, caspase-1, IL-18, pro-IL-1β, and IL-1β were greatly inhibited by FA gels on day 21 and 28, indicating the anti-inflammatory effect of FA gel. Furthermore, the effect of FA gel on the activation of the NLRP3 inflammasome and the expression of downstream inflammatory factors in skin tissues after 40 Gy radiation were investigated using western blotting (Fig. 6F-I) and IHC staining methods (Fig. 6J-K). Treatment with 5%, 10%, and 15% FA gels significantly inhibited the remarkable activation of the NLRP3 inflammasome and the expression of inflammation factors after radiation in the protein level (Fig. 6F-I). The expression of NLRP3 in skin tissue, evaluated through IHC staining (Fig. 6J-K), showed similar findings to the results of western blotting. The expression of NLRP3 and downstream inflammation factors in group Aloe were not statistically different from group 5%, 10%, and 15% FA. No significant difference was observed between FA-treated groups and Aloe-treated group in suppression of inflammation factors (Fig. 6).

3.7 Significant increase of ROS, decrease of SOD and cell proliferation caused by 18 Gy radiation were reversed by FA treatmentin vitro.

Radiation-induced ROS production can disrupt the redox balance and cause oxidative damage to the skin. In this study, we observed a remarkable increase in ROS production (Fig. 7A-B) and inhibition of SOD activity (Fig. 7C) in HaCaT cells after 18 Gy radiation. However, treatment with vitamin C or FA solutions significantly suppressed ROS production and the inhibition of SOD activity in HaCaT cells (Fig. 7A-C). Additionally, treatment with vitamin C and FA solutions (50–100 μg/mL) significantly increased cell proliferation after 18 Gy radiation (Fig. 7D).

FA remarkably suppressed the activation of NLRP3 inflammasome caused by 18 gy radiation in vitro

Twenty-four hours after irradiation, the supernatant of HaCaT cells was collected, and the secreted NLRP3 inflammasome, IL-18, pro-IL-1β and IL-1β were measured using the ELISA method. The secretion of NLRP3 inflammasome, IL-18, pro-IL-1β and IL-1β by HaCaT cells was significantly enhanced after 18 Gy radiation compared to the control group (Fig. 7E-H). However, administration of vitamin C and FA solutions markedly suppressed the secretion of these inflammatory factors (Fig. 7E-H). We also investigated the role of FA in the activation of the NLRP3 inflammasome in HaCaT cells after radiation. The protein expression levels of NLRP3, caspase-1, IL-18, pro-IL-1β, and IL-1β were detected

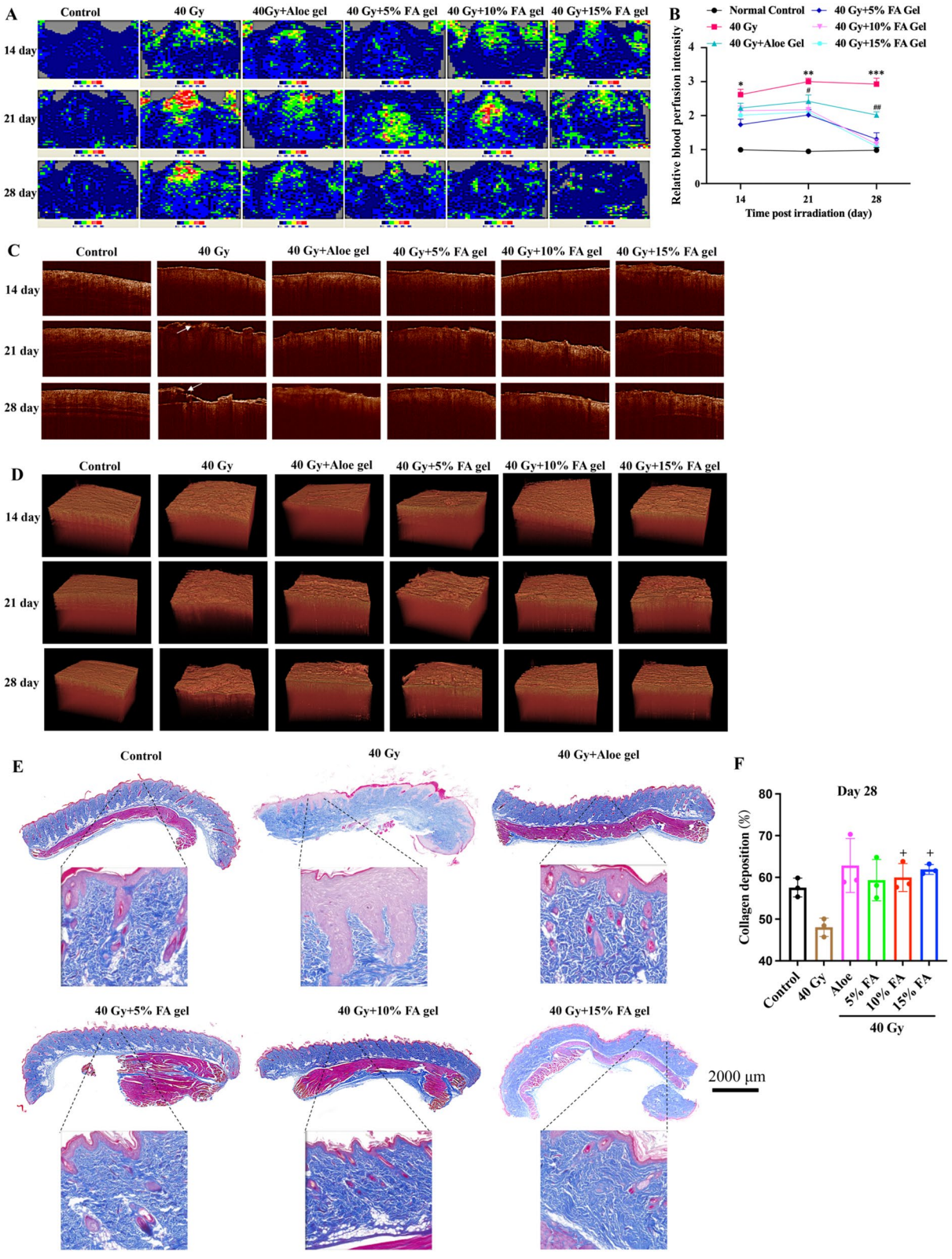

Fig. 5 FA hydrogels reduces rat skin blood flow and promotes skin tissue reconstruction after radiation. (**A**) Recording of skin blood flow in rats using a laser doppler blood flow monitor. (**B**) Quantitative analysis of skin blood flow in rats. (**C**) Evaluation of skin injury using a sweep source OCT system (The white arrow indicates skin injury). (**D**) Three-dimensional OCT imaging analysis. (**E**) Evaluation of collagen deposition using Masson staining on day 28. (**F**) Analysis of collagen deposition. * $p < 0.05$, ** $p < 0.01$, *** $p < 0.001$ compared with the 40 Gy + Aloe gel, 40 Gy + 5% gel, 40 Gy + 10% gel, 40 Gy + 15% gel groups. # $p < 0.05$, ## $p < 0.01$ compared with the 40 Gy + 5% gel, 40 Gy + 10% gel, 40 Gy + 15% gel groups. + $p < 0.05$ compared with group 40 Gy

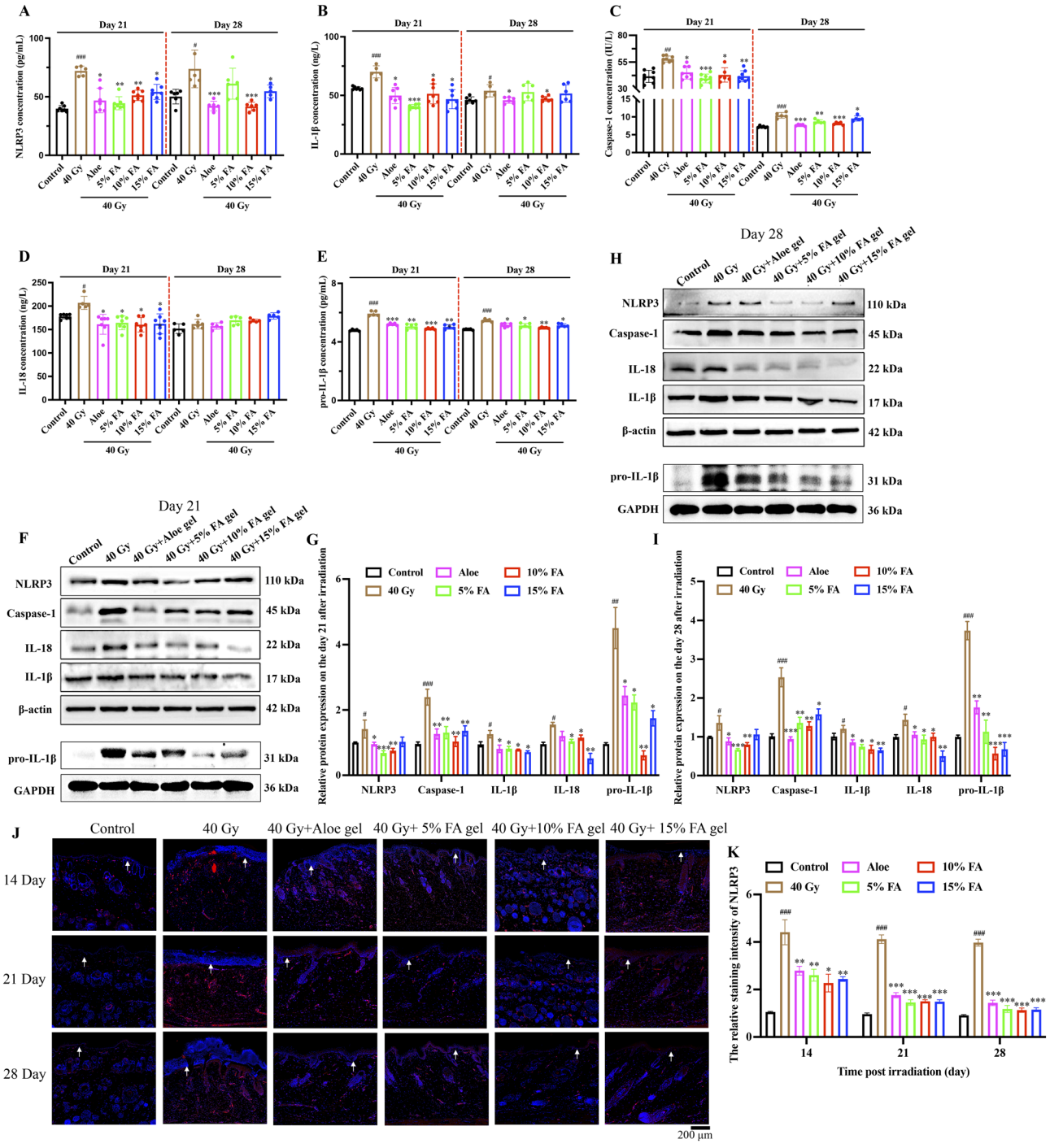

Fig. 6 FA hydrogels suppresses the activation of NLRP3 inflammasome caused by 40 Gy in vivo. (**A**-**E**) Measurement of NLRP3, caspase-1, IL-1β, IL-18, and pro-IL-1β expression in serum of rats 21 and 28 days after radiation. (**F**-**I**) Western blotting analysis of NLRP3, caspase-1, IL-1β, pro-IL-1β, and IL-18 protein expression in skin of rats 21 and 28 days after radiation. (**J**-**K**) Immunohistochemistry staining of NLRP3 expression in dermis and epidermis (White arrows indicate keratinization layer). * $p < 0.05$, ** $p < 0.01$, *** $p < 0.001$ compared with the 40 Gy group. # $p < 0.05$, ## $p < 0.01$, ### $p < 0.001$ compared with the control group

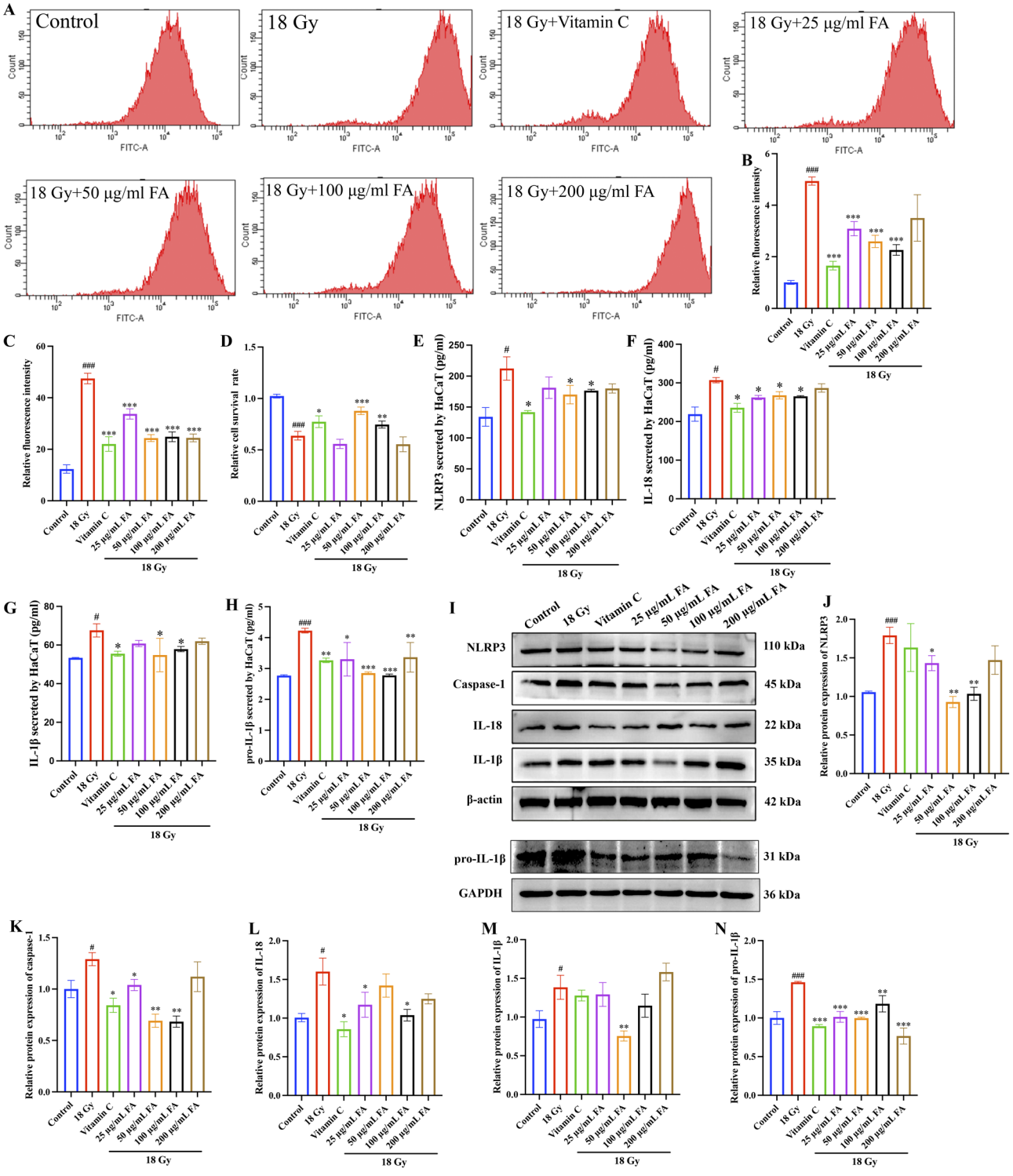

Fig. 7 FA suppresses the activation of NLRP3 inflammasome, increase of ROS, and SOD clearance caused by 18 Gy in vitro. (**A**-**B**) Measurement of ROS production after radiation using flow cytometry. (**C**) Detection of SOD clearance. (**D**) Measurement of cell proliferation after radiation using CCK8 assay. (**E**-**H**) Measurement of NLRP3, IL-1β, pro-IL-1β, IL-18 secretion by cells. (**I**-**N**) Western blotting analysis of NLRP3, caspase-1, IL-1β, pro-IL-1β, IL-18 protein expression in HaCaT cells. * $p < 0.05$, ** $p < 0.01$, *** $p < 0.001$ compared with the 18 Gy group. # $p < 0.05$, ### $p < 0.001$ compared with the control group

using western blotting (Fig. 7I-N). The significant upregulation of NLRP3, caspase-1, IL-18, pro-IL-1β, and IL-1β in HaCaT cells after 18 Gy radiation were greatly decreased by vitamin C or FA solutions (Fig. 7I-N). Thus, FA treatment effectively inhibited the activation of the NLRP3 inflammasome after radiation in vitro.

Transcriptome analysis of HaCaT cells treated with FA post radiation

To investigate the underlying mechanism modulating the alleviation of radiation-induced skin injury by FA, total RNA extracted from HaCaT cells treated or untreated with FA upon radiation was subjected to RNA sequencing. Among the genes with significant expression differences, we screened for genes that were upregulated or downregulated after radiation treatment, but whose expression levels were restored after FA treatment (Fig. 8A). Persistent inflammation and high expression of MMP can delay wound healing [32]. We found that IL-1 A, IL-1B, and MMP14 were significantly overexpressed after radiation, but FA treatment reduced their expression levels (Fig. 8A). In addition, the JAK/STAT pathway is believed to be closely related to chronic wound healing. Through differential gene analysis, we found that the expression of STAT1, STAT3, and STAT6 was inhibited after radiation, while FA activated the STAT pathway to varying degrees (Fig. 8A). The activation of the JAK/STAT pathway may be one of the mechanisms by which FA promotes radiation-induced skin injury healing. In addition, fibroblast growth factor

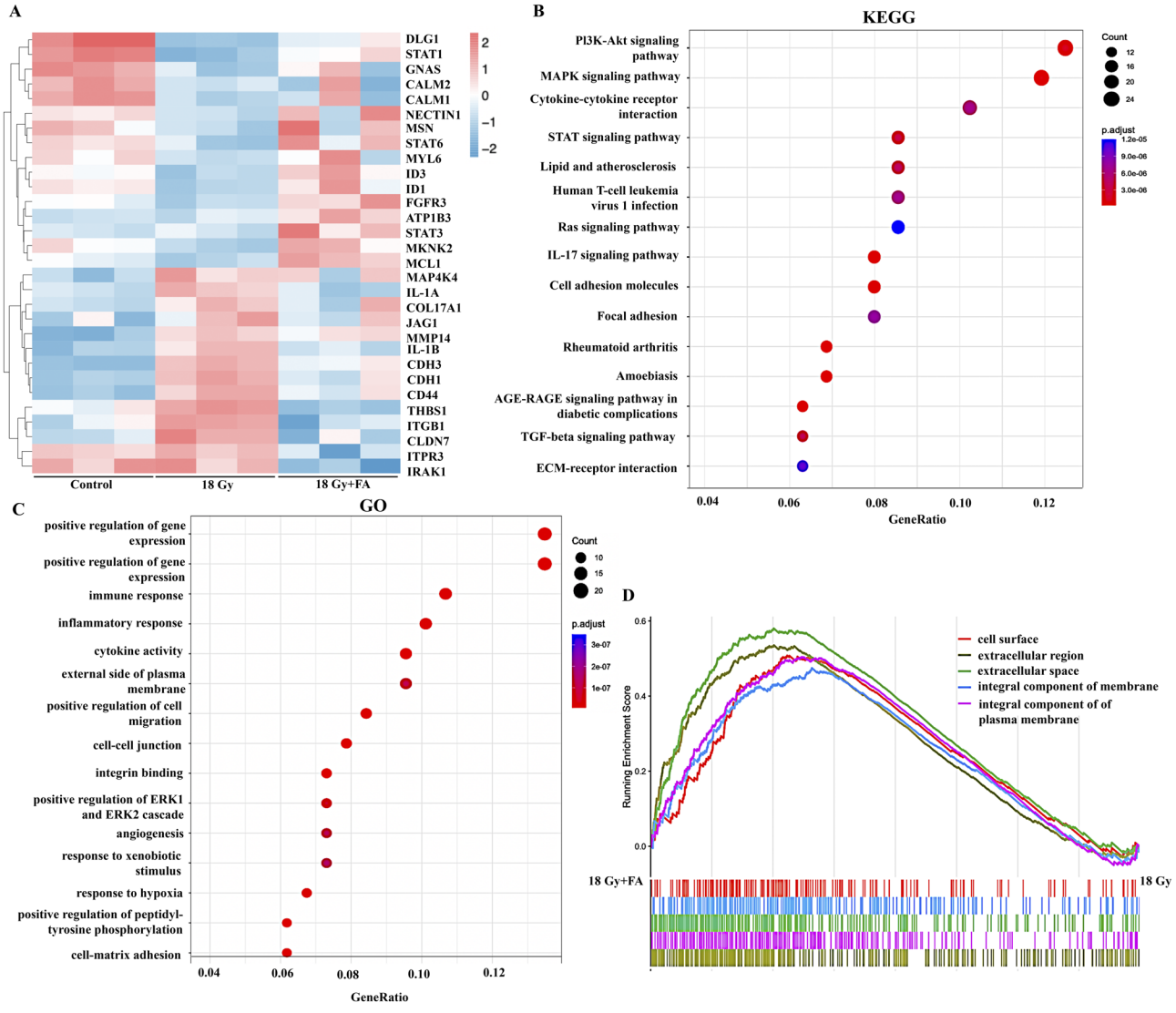

Fig. 8 Transcriptome analysis of HaCaT cells treated with FA post radiation. (**A**) Heatmap for differential expression genes on control, IR, and FA groups with three biological replicate samples for each group. (**B**) KEGG pathway analysis for differential gene expression. (**C**) GO biological process and GO molecular function analysis. (**D**) Gene Set Enrichment Analysis (GSEA) analysis

receptor 3 (FGFR3) is involved in various cellular processes, such as cell growth, angiogenesis, and wound healing [33]. FA significantly promoted its expression (Fig. 8A). Genes upregulated by FA treatment (18 Gy+FA group vs. 18 Gy group) are used for KEGG enrichment. KEGG indicated wound healing process to be implicated within differing pathways, such as STAT, PI3K/AKT, cell adhesion molecules, and TGF-β (Fig. 8B). GO and GSEA analysis suggested radiation exposures affected multiple genes linked with immune response, inflammatory response, cell migration, angiogenesis, hypoxia response, and cell matrix adhesion (Fig. 8C-D).

Discussion

It has been reported that the oral bioavailability of FA is limited (9–20%) due to first-pass metabolism [14, 34]. Hence, we aimed to develop a novel FA gel specifically designed for the treatment of radiation-induced skin injuries. The FA gel we prepared exhibited a uniform and delicate light pink colloid that remained stable at room temperature without drying up or liquefying (Supplementary Fig. 3). The physical and chemical properties of the gel met the quality requirements outlined in the 2020 edition of the Chinese Pharmacopoeia (Part III) [31]. To assess its skin compatibility, we conducted a skin irritation test, and after 72 h of observation, no symptoms of erythema, eschar, or edema formation were observed in the group treated with FA gel, indicating that the prepared gel did not irritate rat skin.

Various forms of FA gel incorporating different materials have been reported in different fields. For instance, a FA-loaded nanoemulsion-based gel was shown to alleviate UVA-induced oxidative stress [14]. Another study prepared FA-loaded nanocapsules using a high-pressure homogenization method [35], although its further application as a gel has not been reported. A triple natural antioxidant hydrogel containing puerarin, ferulic acid, and polydopamine was developed for physical skin wound healing [16]. However, the application of FA hydrogel for radiation injuries has not yet been explored. In our study, we report for the first time the application of a novel FA-embedded carbomer hydrogel for improving radiation-induced skin injuries. Carbomer, commonly used as an adjuvant, serves as a thickener, adhesive, and stabilizer in clinical settings [18].

Hydrogels loaded with active ingredient have been reported to be used in radiation induced skin damage. Injectable multifunctional Schiff base cross-linked with gallic acid modified chitosan/oxidized dextran hydrogels were rationally reported to accelerate wound healing through elimination of ROS in combined radiation and burn injury [27]. Gallic acid-grafted with soy protein and phenol and thiol cohorts combined with graphene oxide could reduce ROS and NLRP3 expression while inhibiting radiation-induced skin injury [36]. Wound healing of radiation-induced skin injury was achieved by mesoporous silica-cerium oxide nanozymes facilitating miR-129 delivery [37]. Interferon-alpha inducible protein 6-based hydrogel promotes the healing of radiation-induced skin injury through regulating heat shock transcription factor 1 [38]. The radiation doses used in these studies ranged from 5 to 30 Gy, while our study use 40 Gy to establish animal model. Higher doses cause more severe skin damage, which suggests the effectiveness of the FA hydrogel in accelerating radiation-induced skin injury.

The anti-radiation role of FA has been widely reported [39–41]. FA presented neuroprotective effect against radiation-induced nerve damage, suggesting that FA might have some potential in the treatment of radiation-induced cognitive impairment [13]. FA accelerate bone defect repair after radiation via maintaining the stemness of skeletal stem cells [42]. The protection effect of testicular after radiation was achieved by FA through regulating SIRT1 and PARP1 [43]. However, the influence of FA on radiation-induced skin injury has not been reported. We demonstrated that our prepared FA gel markedly improved the skin injury caused by 40 Gy by alleviating skin tissue damage, reducing skin blood flow, and inhibiting NLRP3 inflammasome activation. The effects of FA on radiation-induced injury were also validated through in vitro experiments. In addition, reduced ROS level, increased SOD content, and inactivation of NLRP3 inflammasome in HaCaT cells were achieved by FA treatment after 18 Gy radiation induction (Fig. 9).

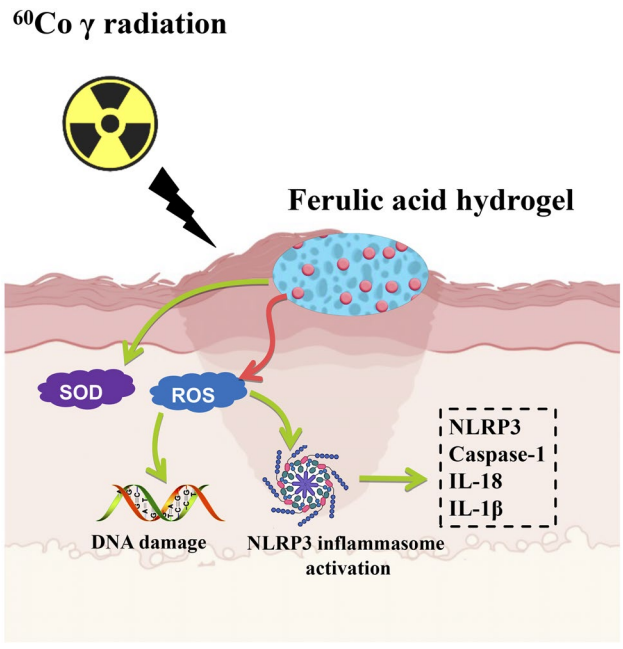

Fig. 9 Scheme of radiation-induced skin injury inhibition by FA hydrogel

The NLRP3 inflammasome is a crucial component of innate immunity and plays a significant role in the body's immune response [44, 45]. Its activation leads to the release of caspase-1, IL-1β, IL-18, and IL-18 outside the cell, further inducing inflammatory reactions or pyroptosis [46, 47]. We observed significant elevations in NLRP3, caspase-1, IL-1β, and IL-18 levels in both serum and skin tissues after 40 Gy radiation, suggesting that FA gel may inhibit radiation-induced skin damage by inactivating the NLRP3 inflammasome. Additionally, IL-1β can directly induce IL-2, recruit neutrophils to enhance the inflammatory cascade response [48], and promote the release of other pro-inflammatory cytokines (TNF-α and IL-6) and chemokines, thereby accelerating the inflammatory response [49, 50]. Consequently, further exploration is needed to investigate the regulation of TNF-α, IL-6, chemokines, and related signaling pathways by FA following radiation. Moreover, after ^{60}Co γ radiation, substantial amounts of ROS and malondialdehyde (MDA) are generated [51], while SOD levels decrease, leading to an imbalance in skin redox and subsequent oxidative cell toxicity [52, 53]. In our research, FA significantly suppressed the increased ROS levels and inhibited SOD activity in vitro (Fig. 7). This mechanism could be one of the ways FA mitigates radiation-induced skin damage (Fig. 9).

Transcriptome analysis indicated that 18 Gy radiation reduced the expression of STAT1, STAT3, and STAT6, which are downstream signals of inflammation. This phenomenon confuses us. Further literature research has found that the regulatory role of STAT family molecules in inflammation and tumors is complex. Research has confirmed that the STAT family can also exert anti-inflammatory effects. It was reported that IFN-I via STAT1 exerted suppressive activity on NLRP1 and NLRP3 inflammasomes, and further inhibited caspase 1 to process the IL1-β precursor [54]. Meanwhile, STAT1 target gene products directly repressed NLRP3 inflammasomes [55]. In addition, STAT1 increased IL-10 synthesis, which is an anti-inflammation cytokine, and suppressed the synthesis of IL1-β precursor [56] In the present study, NLRP3 inflammasome activation was observed after radiation, and down-regulation of STAT1 was found via transcriptome sequencing analysis. The activation of NLRP3 inflammasome after radiation might be regulated by down-regulation of STAT1, which is in line with previous report [55]. In addition, radiation can induce tumor development, and in this study, 18 Gy radiation reduced the expression of STAT1, STAT3, and STAT6. STAT3 and STAT6 are believed to promote the occurrence and development of tumors, while STAT1 is considered a tumor suppressor molecule. These findings indicate that the regulatory role of STAT/JAK pathway in radiation-induced skin injury is complex and requires further exploration.

In this study, we found that all 5%, 10%, and 15% FA hydrogels have good biocompatibility and ROS inhibition ability. All three FA hydrogels were effective in ameliorating radiation-induced skin damage and inhibiting NLRP3 inflammasome activation, but there was no statistical difference among the three groups. In terms of inhibition of NLRP3 (Fig. 6A), caspase-1 (Fig. 6C), and pro-IL-1β (Fig. 6E) in vivo, 10% FA hydrogel was the most effective. Meanwhile, 10% FA hydrogels have the best mechanical strength compared with 5% FA and 15 FA. Therefore, 10% FA hydrogel might be the most ideal concentration. However, at both in vivo and in vitro levels, the dispersed trend of inhibition of NLRP3, caspase-1, IL-18, IL-1β, and pro-IL-1β with increased concentrations of FA was observed. We guess that the optimal dose was not covered by the doses we chose, which is a limitation of this study. We will further screen the optimal dosage in future research. Theoretically, after FA treatment, the levels of NLRP3, caspase-1, IL-18, pro-IL-1β, and IL-1β should be lower on day 28 than on day 21. However, we found that on the 28th day, only the concentration of caspase-1 was lower than on the 21st day. This may be due to different reagents and experimental batches. In addition, this also indicates that the ongoing inflammatory process 28 days after radiation.

Conclusion

In conclusion, we successfully prepared an FA hydrogel by crosslinking FA with carbomer 940. The synthetic hydrogel, crosslinked with 5%, 10%, or 15% FA, effectively alleviated 40 Gy ^{60}Co γ radiation-induced skin injuries. The FA hydrogel significantly reduced skin blood flow, inflammation, oxidative stress, and promoted skin tissue reconstruction and collagen deposition. Moreover, we observed the inactivation of the NLRP3 inflammasome by the FA hydrogel at both in vivo and in vitro levels, suggesting it may be a potential mechanism of action. However, further exploration is necessary to determine the optimal concentration of FA hydrogel and to investigate the specific signaling pathways it targets. The novel FA hydrogel we developed could serve as a promising adjunctive therapy to mitigate radiotherapy-induced skin injuries.

Abbreviations

FA	Ferulic acid
ROS	Reactive oxygen species
SOD	Superoxide dismutase
HE	Hematoxylin and eosin
MDA	Malondialdehyde
HaCaT	Human keratinocytes
OCT	Optical coherence tomography
TEM	Transmission electron microscopy
PBS	Phosphate buffered saline
BCA	Bicinchoninic acid
PVDF	Polyvinylidene fluoride
TBST	Tris buffered saline with tween

FPKM	Fragments per kilo base per million mapped reads
H_2O_2	Hydrogen peroxide

Supplementary Information

The online version contains supplementary material available at https://doi.org/10.1186/s12951-024-02789-7.

Supplementary Material 1

Supplementary Material 2

Supplementary Material 3

Supplementary Material 4

Supplementary Material 5

Acknowledgements
Not applicable.

Author contributions
ZM, WZ, CH, and YG conceived and designed the experiments; CH, CH, WZ, LZ, ZB, PS, GL, HD, and NW performed the experiments; CH and CH wrote the paper. All data were generated in-house, and no paper mill was used. All authors agree to be accountable for all aspects of work ensuring integrity and accuracy.

Funding
This research was funded by National Key Research and Development Program (2022YFC3500303), Innovation Team and Talents Cultivation Program of National Administration of Traditional Chinese Medicine (ZYYCXTD-C-202009 and ZYYCXTD-D-202207), National Natural Science Foundation of China (81873063).

Data availability
The data and material used to support the findings of this study are included within the manuscript and supplementary files.

Declarations

Ethical approval and consent to participate
The experimental protocol was approved by the Ethics Committee of Animal Experiments of the Beijing Institute of Radiation Medicine.

Consent for publication
Not applicable.

Competing interests
The authors declare no competing interests.

Author details
[1]Department of Pharmaceutical Sciences, Beijing Institute of Radiation Medicine, No. 27 Taiping Road, Beijing 100850, China
[2]State Key Laboratory of Kidney Diseases, Chinese PLA General Hospital, No. 28 Fuxing Road, Beijing 100853, China
[3]Department of Traditional Chinese medicine, Henan University of Chinese Medicine, No. 156 Jinshui East Road, Zhengzhou 450046, China
[4]Qinghai University, No. 251 Ningda Road, Xining 810016, China

Received: 29 May 2024 / Accepted: 20 August 2024
Published online: 19 September 2024

References

1. Barazzuol L, Coppes RP, van Luijk P. Prevention and treatment of radiotherapy-induced side effects. Mol Oncol. 2020;14(7):1538–54.
2. Huang C, Zhang L, Shen P, Wu Z, Li G, Huang Y, et al. Cannabidiol mitigates radiation-induced intestine ferroptosis via facilitating the heterodimerization of RUNX3 with CBFbeta thereby promoting transactivation of GPX4. Free Radic Biol Med. 2024;222:288–303.
3. Yao C, Zhou Y, Wang H, Deng F, Chen Y, Zhu X, et al. Adipose-derived stem cells alleviate radiation-induced dermatitis by suppressing apoptosis and downregulating cathepsin F expression. Stem Cell Res Ther. 2021;12(1):447.
4. Huangfu C, Tang N, Yang X, Gong Z, Li J, Jia J, et al. Improvement of irradiation-induced fibroblast damage by alpha2-macroglobulin through alleviating mitochondrial dysfunction. Pharm Biol. 2022;60(1):1365–73.
5. Bray FN, Simmons BJ, Wolfson AH, Nouri K. Acute and chronic cutaneous reactions to Ionizing Radiation Therapy. Dermatol Ther (Heidelb). 2016;6(2):185–206.
6. Xiao Y, Mo W, Jia H, Yu D, Qiu Y, Jiao Y, et al. Ionizing radiation induces cutaneous lipid remolding and skin adipocytes confer protection against radiation-induced skin injury. J Dermatol Sci. 2020;97(2):152–60.
7. Zhou L, Huang C, HuangFu C, Shen P, Hu Y, Wang N, et al. Low-dose radiation-induced SUMOylation of NICD1 negatively regulates osteogenic differentiation in BMSCs. Ecotoxicol Environ Saf. 2024;282:116655.
8. Singh M, Alavi A, Wong R, Akita S, Radiodermatitis. A review of our current understanding. Am J Clin Dermatol. 2016;17(3):277–92.
9. Zdunska K, Dana A, Kolodziejczak A, Rotsztejn H. Antioxidant properties of Ferulic Acid and its possible application. Skin Pharmacol Physiol. 2018;31(6):332–6.
10. Antonopoulou I, Sapountzaki E, Rova U, Christakopoulos P. Ferulic Acid from Plant Biomass: a Phytochemical with Promising Antiviral properties. Front Nutr. 2021;8:777576.
11. Wang YL, Wang WK, Wu QC, Yang HJ. The release and catabolism of ferulic acid in plant cell wall by rumen microbes: a review. Anim Nutr. 2022;9:335–44.
12. Chen Y, Shen J, Zhang X, Gao W, Cao Q, Yan F, et al. Protective effects of ferulic acid against ionizing radiation-induced oxidative damage in rat lens through activating Nrf2 signal pathway. Int J Ophthalmol. 2023;16(5):687–93.
13. Liu G, Nie Y, Huang C, Zhu G, Zhang X, Hu C, et al. Ferulic acid produces neuroprotection against radiation-induced neuroinflammation by affecting NLRP3 inflammasome activation. Int J Radiat Biol. 2022;98(9):1442–51.
14. Harwansh RK, Mukherjee PK, Bahadur S, Biswas R. Enhanced permeability of ferulic acid loaded nanoemulsion based gel through skin against UVA mediated oxidative stress. Life Sci. 2015;141:202–11.
15. Liang Y, He J, Guo B. Functional hydrogels as Wound Dressing to Enhance Wound Healing. ACS Nano. 2021;15(8):12687–722.
16. Ou Q, Zhang S, Fu C, Yu L, Xin P, Gu Z, et al. More natural more better: triple natural anti-oxidant puerarin/ferulic acid/polydopamine incorporated hydrogel for wound healing. J Nanobiotechnol. 2021;19(1):237.
17. Tan D, Zhu W, Liu L, Pan Y, Xu Y, Huang Q, et al. In situ formed scaffold with royal jelly-derived extracellular vesicles for wound healing. Theranostics. 2023;13(9):2811–24.
18. Guan M, Chu G, Jin J, Liu C, Cheng L, Guo Y et al. A combined Cyanine/Carbomer gel enhanced photodynamic antimicrobial activity and Wound Healing. Nanomaterials (Basel). 2022;12(13).
19. Chen CY, Yin H, Chen X, Chen TH, Liu HM, Rao SS, et al. Angstrom-scale silver particle-embedded carbomer gel promotes wound healing by inhibiting bacterial colonization and inflammation. Sci Adv. 2020;6:43.
20. Albrecht S, Jung S, Muller R, Lademann J, Zuberbier T, Zastrow L, et al. Skin type differences in solar-simulated radiation-induced oxidative stress. Br J Dermatol. 2019;180(3):597–603.
21. Li W, Du D, Huang Y, Xu C, Liu Y, Wu X, et al. Improvement of skin wound healing by giant salamander skin mucus gel wrapped with bone marrow mesenchymal stem cells via affecting integrin family molecules. Aging. 2024;16(9):7902–14.
22. Liu YG, Chen JK, Zhang ZT, Ma XJ, Chen YC, Du XM, et al. NLRP3 inflammasome activation mediates radiation-induced pyroptosis in bone marrow-derived macrophages. Cell Death Dis. 2017;8(2):e2579.
23. Wang X, Li X, Liu J, Tao Y, Wang T, Li L. Lactobacillus Plantarum promotes Wound Healing by inhibiting the NLRP3 inflammasome and pyroptosis activation in Diabetic Foot wounds. J Inflamm Res. 2024;17:1707–20.
24. Huang W, Jiao J, Liu J, Huang M, Hu Y, Ran W, et al. MFG-E8 accelerates wound healing in diabetes by regulating NLRP3 inflammasome-neutrophil extracellular traps axis. Cell Death Discov. 2020;6:84.
25. Ito H, Kanbe A, Sakai H, Seishima M. Activation of NLRP3 signalling accelerates skin wound healing. Exp Dermatol. 2018;27(1):80–6.
26. Liu C, Yu Q, Yuan Z, Guo Q, Liao X, Han F, et al. Engineering the viscoelasticity of gelatin methacryloyl (GelMA) hydrogels via small dynamic bridges to regulate BMSC behaviors for osteochondral regeneration. Bioact Mater. 2023;25:445–59.

27. Shen J, Jiao W, Chen Z, Wang C, Song X, Ma L, et al. Injectable multifunctional chitosan/dextran-based hydrogel accelerates wound healing in combined radiation and burn injury. Carbohydr Polym. 2023;316:121024.
28. Foubert P, Doyle-Eisele M, Gonzalez A, Berard F, Weber W, Zafra D, et al. Development of a combined radiation and full thickness burn injury minipig model to study the effects of uncultured adipose-derived regenerative cell therapy in wound healing. Int J Radiat Biol. 2017;93(3):340–50.
29. Chuchvara N, Rao B, Liu X. Manually scanned single fiber optical coherence tomography for skin cancer characterization. Sci Rep. 2021;11(1):15570.
30. Ferreira JA. The Benjamini-Hochberg method in the case of discrete test statistics. Int J Biostat. 2007;3(1):Article11.
31. Commission NP. Pharmacopoeia of the people's Republic of China (2020). Beijing: China Medical Science Press; 2020.
32. Schilrreff P, Alexiev U. Chronic inflammation in non-healing skin wounds and Promising Natural Bioactive compounds Treatment. Int J Mol Sci. 2022;23(9).
33. Chakraborty D, Zhu H, Jungel A, Summa L, Li YN, Matei AE et al. Fibroblast growth factor receptor 3 activates a network of profibrotic signaling pathways to promote fibrosis in systemic sclerosis. Sci Transl Med. 2020;12(563).
34. Bourne LC, Rice-Evans C. Bioavailability of ferulic acid. Biochem Biophys Res Commun. 1998;253(2):222–7.
35. Das S, Wong ABH. Stabilization of ferulic acid in topical gel formulation via nanoencapsulation and pH optimization. Sci Rep. 2020;10(1):12288.
36. Daijun Zhou HL, Lu Han D, Liu X, Liu Q, He YD, Li ZH, Lu X, Jiang C. Dong Li. Paintable graphene oxide-hybridized soy protein-based biogels for skin radioprotection. Chem Eng J. 2023;469(143914):1–12.
37. Zhou D, Du M, Luo H, Ran F, Zhao X, Dong Y, et al. Multifunctional mesoporous silica-cerium oxide nanozymes facilitate miR129 delivery for high-quality healing of radiation-induced skin injury. J Nanobiotechnol. 2022;20(1):409.
38. Hao J, Sun M, Li D, Zhang T, Li J, Zhou D. An IFI6-based hydrogel promotes the healing of radiation-induced skin injury through regulation of the HSF1 activity. J Nanobiotechnol. 2022;20(1):288.
39. Shao S, Gao Y, Liu J, Tian M, Gou Q, Su X. Ferulic acid mitigates Radiation Injury in Human umbilical vein endothelial cells in Vitro via the Thrombomodulin Pathway. Radiat Res. 2018;190(3):298–308.
40. Srinivasan M, Sudheer AR, Pillai KR, Kumar PR, Sudhakaran PR, Menon VP. Influence of ferulic acid on gamma-radiation induced DNA damage, lipid peroxidation and antioxidant status in primary culture of isolated rat hepatocytes. Toxicology. 2006;228(2–3):249–58.
41. Das U, Manna K, Sinha M, Datta S, Das DK, Chakraborty A, et al. Role of ferulic acid in the amelioration of ionizing radiation induced inflammation: a murine model. PLoS ONE. 2014;9(5):e97599.
42. Liang JW, Li PL, Wang Q, Liao S, Hu W, Zhao ZD, et al. Ferulic acid promotes bone defect repair after radiation by maintaining the stemness of skeletal stem cells. Stem Cells Transl Med. 2021;10(8):1217–31.
43. El-Mesallamy HO, Gawish RA, Sallam AM, Fahmy HA, Nada AS. Ferulic acid protects against radiation-induced testicular damage in male rats: impact on SIRT1 and PARP1. Environ Sci Pollut Res Int. 2018;25(7):6218–27.
44. Moretti J, Jia B, Hutchins Z, Roy S, Yip H, Wu J, et al. Caspase-11 interaction with NLRP3 potentiates the noncanonical activation of the NLRP3 inflammasome. Nat Immunol. 2022;23(5):705–17.
45. Zou J, Yang R, Feng R, Liu J, Wan JB. Ginsenoside Rk2, a dehydroprotopanaxadiol saponin, alleviates alcoholic liver disease via regulating NLRP3 and NLRP6 inflammasome signaling pathways in mice. J Pharm Anal. 2023;13(9):999–1012.
46. Huang Y, Xu W, Zhou R. NLRP3 inflammasome activation and cell death. Cell Mol Immunol. 2021;18(9):2114–27.
47. Seoane PI, Lee B, Hoyle C, Yu S, Lopez-Castejon G, Lowe M et al. The NLRP3-inflammasome as a sensor of organelle dysfunction. J Cell Biol. 2020;219(12).
48. Jain A, Irizarry-Caro RA, McDaniel MM, Chawla AS, Carroll KR, Overcast GR, et al. T cells instruct myeloid cells to produce inflammasome-independent IL-1beta and cause autoimmunity. Nat Immunol. 2020;21(1):65–74.
49. Menoret A, Buturla JA, Xu MM, Svedova J, Kumar S, Rathinam VAK, et al. T cell-directed IL-17 production by lung granular gammadelta T cells is coordinated by a novel IL-2 and IL-1beta circuit. Mucosal Immunol. 2018;11(5):1398–407.
50. Zheng D, Liwinski T, Elinav E. Inflammasome activation and regulation: toward a better understanding of complex mechanisms. Cell Discov. 2020;6:36.
51. Ahmad S, Hussain A, Ullah F, Jamil M, Ali A, Ali S et al. 60Co-gamma Radiation alters Developmental stages of Zeugodacus cucurbitae (Diptera: Tephritidae) through apoptosis pathways Gene expression. J Insect Sci. 2021;21(5).
52. Yi J, Chen C, Liu X, Kang Q, Hao L, Huang J, et al. Radioprotection of EGCG based on immunoregulatory effect and antioxidant activity against (60)cogamma radiation-induced injury in mice. Food Chem Toxicol. 2020;135:111051.
53. Freitinger Skalicka Z, Zolzer F, Beranek L, Racek J. Indicators of oxidative stress after ionizing and/or non-ionizing radiation: superoxid dismutase and malondialdehyde. J Photochem Photobiol B. 2012;117:111–4.
54. Tschopp J, Schroder K. NLRP3 inflammasome activation: the convergence of multiple signalling pathways on ROS production? Nat Rev Immunol. 2010;10(3):210–5.
55. Rauch I, Muller M, Decker T. The regulation of inflammation by interferons and their STATs. JAKSTAT. 2013;2(1):e23820.
56. Guarda G, Braun M, Staehli F, Tardivel A, Mattmann C, Forster I, et al. Type I interferon inhibits interleukin-1 production and inflammasome activation. Immunity. 2011;34(2):213–23.

Publisher's note